PHYSICAL REVIEW D **90,** 074034 (2014)

Dynamical three-field AdS/QCD model

Sean P. Bartz and Joseph I. Kapusta

School of Physics and Astronomy, University of Minnesota, Minneapolis, Minnesota 55455, USA

(Received 16 June 2014; published 30 October 2014)

The AdS/CFT correspondence may offer new and useful insights into the nonperturbative regime of strongly coupled gauge theories such as QCD. We present an AdS/CFT-inspired model that describes the spectra of light mesons. The conformal symmetry is broken by a background dilaton field, and chiral symmetry breaking and linear confinement are described by a chiral condensate field. These background fields, along with a background glueball condensate field, are derived from a potential. We describe the construction of the potential, and the calculation of the meson spectra, which match experimental data well. We argue that the presence of the third background field is necessary to properly describe the meson spectra.

DOI: 10.1103/PhysRevD.90.074034 PACS numbers: 14.40.Be, 11.25.Tq, 12.40.-y

I. INTRODUCTION

The AdS/CFT correspondence is a useful mathematical tool for the analysis of strongly coupled gauge theories. This correspondence establishes a connection between a d-dimensional super Yang Mills theory and a weakly coupled gravitational theory in $d+1$ dimensions [1–3]. Calculations that are analytically intractable in the field theory can be related to results from the gravity theory using an effective dictionary developed over the past decade. QCD is a strongly coupled gauge theory at hadronic scales, making it a candidate for the application of the gauge/gravity correspondence. It is not known whether a gravitational dual to QCD exists, but there has been much work on models that capture its key features. The bottom-up approach assumes the existence of such a dual, modeling features of QCD by an effective five-dimensional gravity theory. Linear confinement in QCD sets a scale that is encoded in a cutoff of the fifth dimension in the anti–de Sitter (AdS)/QCD model [4,5]. So-called soft-wall models use a dilaton field as an effective cutoff to limit the penetration of the meson fields into the bulk [6]. The simplest soft-wall models use a quadratic dilaton to recover the linear Regge trajectories, while models that modify the UV behavior of the dilaton more accurately model the ground-state masses [7–10].

The soft-wall models typically include at least two background fields: the aforementioned dilaton, and a chiral condensate field that corresponds to the chiral symmetry breaking in the gauge theory. These models use parametrizations for the background dilaton and chiral fields that are not derived as the solution to any equations of motion. A well-defined action would provide a set of background equations from which these fields can be derived, and may suggest how the model can be derived from a top-down approach. In addition, this action provides access to the thermal properties of the model through perturbation of the geometry [11–13].

In this paper, we expand upon previous work to find a suitable potential for the background fields of a soft-wall AdS/QCD model [13–20]. After demonstrating the limitations of models including a dilaton and chiral field alone, we suggest the inclusion of a background glueball field. We then construct a potential that satisfies the necessary UV and IR limits, and use this potential to generate numerically the background fields and calculate the resulting meson spectra.

II. REVIEW AND MOTIVATION

We assume that four-dimensional QCD can be modeled by the following five-dimensional action, written in the string frame:

$$\mathcal{S} = \frac{1}{16\pi G_5}\int d^5x\sqrt{-g}e^{-2\Phi}\Big(R + 4\partial_M\Phi\partial^M\Phi - \mathrm{Tr}\Big[|DX|^2 + \partial_M\mathcal{G}\partial^M\mathcal{G} + \frac{1}{2g_5^2}(F_A^2 + F_V^2) + V_m(\Phi, X^2, \mathcal{G})\Big]\Big). \tag{1}$$

Here Φ is the dilaton and the metric is pure AdS, $g_{MN} = z^{-2}\eta_{MN}$, with the AdS curvature defined to be unity. The constant $g_5^2 = 12\pi^2/N_c$, where N_c is the number of colors. The covariant derivative is defined as $D_M = \partial_M + i[V_M, X] - i\{A_M, X\}$. The scalar field X, which is dual to the $\bar{q}q$ operator, obtains a z-dependent vacuum expectation value (VEV),

$$\langle X\rangle = \frac{\chi(z)}{2}I, \tag{2}$$

where I is the 2×2 identity matrix. The glueball field $\mathcal{G}$ similarly obtains a z-dependent VEV, $G(z)$. We examine the background dynamics of the fields

$$\mathcal{S} = \frac{1}{16\pi G_5}\int d^5x\sqrt{-g}e^{-2\Phi}\Big(R + 4\partial_M\Phi\partial^M\Phi - \frac{1}{2}\partial_M\chi\partial^M\chi - \frac{1}{2}\partial_M G\partial^M G - V(\Phi,\chi,G)\Big), \quad (3)$$

where $V = \mathrm{Tr}[V_m]$. The scalar fields Φ, χ, G are dimensionless.

It is easier to search for the background fields in the Einstein frame, where the vacuum action takes the canonical form

$$\mathcal{S}_E = \frac{1}{16\pi G_5}\int d^5x\sqrt{-\tilde{g}}\Big(\tilde{R} - \frac{1}{2}\partial_M\phi\partial^M\phi - \frac{1}{2}\partial_M\chi\partial^M\chi - \frac{1}{2}\partial_M G\partial^M G - \tilde{V}(\phi,\chi,G)\Big). \quad (4)$$

The tilde distinguishes the two frames, with $\tilde{V} = e^{4\Phi/3}V$, and the dilaton is rescaled for a canonical action $\phi = \sqrt{8/3}\Phi$. The string and Einstein-frame metrics are related by the conformal transformation

$$g_{MN} = e^{2\phi/\sqrt{6}}\tilde{g}_{MN}. \quad (5)$$

Previous work showed how to construct a potential for a gravity-dilaton-chiral system without the glueball condensate. We examine the behavior assuming that the fields have a power-law behavior, which is accurate in both the UV and IR limits [15]. One of the equations of motion is independent of the choice of potential,

$$\dot{\chi}^2 = \frac{\sqrt{6}}{z^2}\frac{d}{dz}(z^2\dot{\phi}). \quad (6)$$

Here, the dot represents differentiation with respect to the z coordinate. To obtain linear confinement, the dilaton should have quadratic behavior in the IR limit, $\Phi(z) = \lambda z^2$. The chiral field should have linear behavior in the IR, $\chi(z) = Az$, where A sets the mass splitting between the axial-vector and vector mesons for large radial quantum numbers n. This constant mass splitting at large n occurs because of the nonrestoration of chiral symmetry [21]. Inserting this IR behavior for the dilaton and chiral field into Eq. (6), we find that the chiral field behaves as

$$\chi(z\to\infty) = 2\sqrt{6\lambda}z, \quad (7)$$

linking the IR behavior of the chiral condensate with the parameter that determines the radial Regge trajectories. However, the IR behavior of the chiral field determines the constant mass splitting between the axial-vector and vector mesons for large radial quantum numbers n [7],

$$\Delta m^2 \equiv (m^2_{A_n} - m^2_{V_n})_{n\to\infty} = \frac{g_5^2}{z^2}\chi^2(z\to\infty) = 24g_5^2\lambda. \quad (8)$$

Thus, there is no independent parameter in the model that controls this mass splitting. Using the value of $\lambda = 0.1831/2$ GeV^2 found Ref. [7] (our definition of λ differs from theirs by a factor of 2), we find a value for $\Delta m^2 = 87$ GeV^2, which is much larger than the experimental value of 1.42 GeV^2. Because this problem arises in the equation that is independent of the potential, it cannot be resolved by the choice of potential in models that do not consider the glueball condensate. Models that derive the field behavior using the superpotential method suffer from the same problem.

To resolve this problem, we consider the effects of the glueball condensate G on the background equations. This field must be linear in the IR for linear confinement, and behave as $G\sim z^4$ in the UV to match the operator dimension in the AdS/CFT dictionary.

It is noted that the model proposed by Huang and Li [18,19] accurately represents the nonrestoration of chiral symmetry using a model with only two background fields, but their model differs from the work presented here in several respects. They place the meson fields and chiral dynamics in the open-string sector of the model. For linear confinement, this requires that the chiral field approach a constant in the IR, which necessitates a modified metric to obtain the correct chiral dynamics. Our model allows the metric to remain purely AdS in the string frame. Finally, they do not determine an explicit form of the potential, which is the central goal of this work.

III. CONSTRUCTION OF POTENTIAL

Consider the action in the Einstein frame (4). To simplify the equations of motion, we use a transformed potential,

$$V = e^{-2\phi/\sqrt{6}}\tilde{V}. \quad (9)$$

This is simply the potential in the string frame. We rewrite it as

$$V = -12 + 4\sqrt{6}\phi + a_0\phi^2 + \frac{m_X^2}{2}\chi^2 + U. \quad (10)$$

Here U is more than quadratic in the fields. The AdS/CFT dictionary sets the mass for the fields according to the dimension of the dual operator,

$$m^2L^2 = \Delta(\Delta - 4), \quad (11)$$

where L is the AdS curvature which we set to unity. The dimension of the $q\bar{q}$ operator is three, so $m_X^2 = -3/L^2$. The dilaton mass is undetermined and is not connected to the dimension of the corresponding operator, as discussed in Ref. [15]. It is related to the parameter a_0 by $a_0 = \frac{1}{2}[(m_\phi L)^2 2 - 8]$. The potential should be an even function of χ.

The equations of motion can be written as

$$\dot{\chi}^2 + \dot{G}^2 = \frac{\sqrt{6}}{z^2}\frac{d}{dz}(z^2\dot{\phi}), \tag{12}$$

$$U = \frac{1}{2}\sqrt{6}z^2\ddot{\phi} - \frac{3}{2}(z\dot{\phi})^2 - 3\sqrt{6}z\dot{\phi} - 4\sqrt{6}\phi - a_0\phi^2 + \frac{3}{2}\chi^2, \tag{13}$$

$$\frac{\partial U}{\partial \phi} = 3z\dot{\phi} - 2a_0\phi, \tag{14}$$

$$\frac{\partial U}{\partial \chi} = z^2\ddot{\chi} - 3z\dot{\chi}\left(1 + \frac{z\dot{\phi}}{\sqrt{6}}\right) + 3\chi, \tag{15}$$

$$\frac{\partial U}{\partial G} = z^2\ddot{G} - 3z\dot{G}\left(1 + \frac{z\dot{\phi}}{\sqrt{6}}\right). \tag{16}$$

We assume that the potential has no explicit dependence on the coordinate z, so Eqs. (14)–(16) are not independent, and we can eliminate one.

A. Infrared limit

The requirement of linear confinement requires a solution in the large-z limit of the form

$$\phi = \sqrt{\frac{8}{3}}\lambda z^2, \tag{17}$$

$$\chi = Az, \tag{18}$$

$$G = Bz. \tag{19}$$

Substituting this into Eq. (12) gives

$$A^2 + B^2 = 24\lambda. \tag{20}$$

The parameter λ is fixed by the slope of the linear trajectory and A is fixed by the axial vector–vector mass difference. It is useful to write these as

$$A = 2\sqrt{6\lambda}\cos\theta, \quad B = 2\sqrt{6\lambda}\sin\theta, \tag{21}$$

where θ now becomes the parameter controlling the axial vector–vector mass splitting. Inserting Eq. (19) into Eqs. (13)–(16) suggests the following terms in our ansatz for the potential:

$$U = a_1\phi\chi^2 + a_2\phi G^2 + a_3\chi^4 + a_4G^4 + a_5\chi^2G^2 + a_6G^2\tanh(g\phi). \tag{22}$$

We see that there must be a G^2 term in the IR limit, but this is forbidden in the weak-field limit because the glueball condensate field is massless. To circumvent this, we propose the term $G^2\tanh(g\phi)$ with $g > 0$. In the weak-field limit this goes to $g\phi G^2$, which is acceptable. The tanh is suggested by Eq. (9), and it provides a rapid exponential transition from the weak-field to the strong-field limit that is supported by phenomenology. By substitution one finds the following constraints on the parameters:

$$U \to 6 + a_0 + 6\sqrt{6}(\cos^2\theta a_1 + \sin^2\theta a_2), + 6^3(\cos^4\theta a_3 + \sin^4\theta a_4 + \cos^2\theta\sin^2\theta a_5) = 0, \tag{23}$$

$$\frac{\partial U}{\partial \chi} \to 2a_1 + 24\sqrt{6}\cos^2\theta a_3 + 12\sqrt{6}\sin^2\theta a_5 + \sqrt{6} = 0, \tag{24}$$

$$\frac{\partial U}{\partial G} \to 2a_2 + 24\sqrt{6}\sin^2\theta a_4 + 12\sqrt{6}\cos^2\theta a_5 + \sqrt{6} = 0, \tag{25}$$

$$\frac{\partial U}{\partial G} \to a_6 = -\frac{3}{2}. \tag{26}$$

We have chosen to exclude Eq. (14) because it is not independent. The parameter a_6 is determined, and the others will be determined by an examination of the UV limit.

B. Ultraviolet limit

Next we look for a solution in the small-z limit. The AdS/CFT dictionary dictates that the leading-order UV behavior of the chiral and glueball condensate fields is determined by their dimension. Note also that we are working in the chiral limit where the quark mass is zero. We start by examining only the leading-order terms,

$$\chi = \Sigma_0 z^3, \tag{27}$$

$$G = G_0 z^4. \tag{28}$$

Substituting this into Eq. (12) and imposing the boundary condition $\phi(0) = 0$ gives

$$\phi = \frac{\sqrt{6}}{28}\Sigma_0^2 z^6 + \frac{\sqrt{6}}{27}G_0^2 z^8. \tag{29}$$

Using only this leading-order behavior in Eqs. (13)–(16), the system of equations is inconsistent, as there are more equations from matching powers of z than unknown parameters.

To solve this problem, we consider adding a term $\Sigma_n z^n$ to χ. By substituting this into Eq. (12) and keeping only the lowest-order cross term we find the additional term in ϕ,

$$\Delta\phi = \frac{\sqrt{6}n\Sigma_0\Sigma_n}{(n+4)(n+3)}z^{n+3}. \tag{30}$$

From Eq. (13) we find that

$$U = -\frac{3}{2}(z\dot{\phi})^2 - a_0\phi^2 + 3\frac{n^3 - 13n + 12}{(n+4)(n+3)}\Sigma_0\Sigma_n z^{n+3}. \tag{31}$$

Since the ϕ^2 terms start out as z^{12}, z^{14}, z^{16}, and so do the terms in the potential, the n can only take the values 9, 11, etc. This term contributes only to the equation for $\partial U/\partial\chi$,

$$\frac{\partial U}{\partial\chi} = -9\Sigma_0\left(\frac{3}{14}\Sigma_0^2 + \frac{8}{27}G_0^2z^2\right)z^9 + (n-3)(n-1)\Sigma_n z^n. \tag{32}$$

By power counting both $n = 9$ and $n = 11$ can contribute.

There could also be higher-order terms in G such as $G_m z^m$. This leads to the additional term in ϕ,

$$\Delta\phi = \frac{8mG_0G_m}{\sqrt{6}(m+5)(m+4)}z^{m+4}. \tag{33}$$

It contributes to the equation for $\partial U/\partial G$ as

$$\frac{\partial U}{\partial G} = -12G_0\left(\frac{3}{14}\Sigma_0^2 + \frac{8}{27}G_0^2z^2\right)z^{10} + m(m-4)G_n z^m. \tag{34}$$

The choice $m = 8$ is not possible as there is no term of the same order to balance it. Terms with $m = 10$ and $m = 12$ are possible. These new terms cannot affect the equation for $\partial U/\partial\phi$ nor can they contribute to the equation for $\partial U/\partial\chi$. Considering higher-order terms in both χ and G leads to

$$U = -\frac{3}{2}(z\dot{\phi})^2 - a_0\phi^2 + 3\frac{n^3 - 13n + 12}{(n+4)(n+3)}\Sigma_0\Sigma_n z^{n+3} + \frac{4m(m-4)}{m+4}G_0G_m z^{m+4}. \tag{35}$$

The appearance of these terms can be understood by writing the following schematic expansions:

$$\chi \sim \Sigma_0 z^3 + \Sigma_0^3 z^9 + G_0^2\Sigma_0 z^{11} + \cdots,$$
$$G \sim G_0 z^4 + \Sigma_0^2 G_0 z^{10} + G_0^3 z^{12} + \cdots.$$

That is, χ is an odd function of Σ_0 and G is an odd function of G_0. These are the symmetries in the equations of motion. They also follow the spirit of the AdS/CFT correspondence in terms of the dimensionality of the operators and the powers of z.

Including now $m = 10$ and 12, and $n = 9$ and 11, we have the following set of equations in the small-z limit, where LHS and RHS refer to the left and right sides of the respective equations:

$$U_{\rm LHS} = 3\Sigma_0^4 z^{12}\left[4\frac{\Sigma_9}{\Sigma_0^3} - \frac{(54+a_0)}{2^3\cdot 7^2}\right] + \frac{1}{7}\Sigma_0^2G_0^2z^{14}\left[120\frac{G_{10}}{\Sigma_0^2G_0} + 120\frac{\Sigma_{11}}{\Sigma_0G_0^2} - \frac{(72+a_0)}{9}\right] + 2G_0^4z^{16}\left[12\frac{G_{12}}{G_0^3} - \frac{(96+a_0)}{3^5}\right], \tag{36}$$

$$U_{\rm RHS} = \Sigma_0^4 z^{12}\left[\frac{\sqrt{6}}{28}a_1 + a_3\right] + \Sigma_0^2G_0^2z^{14}\left[\frac{\sqrt{6}}{27}a_1 + \frac{\sqrt{6}}{28}(a_2 + ga_6) + a_5\right] + G_0^4z^{16}\left[\frac{\sqrt{6}}{27}(a_2 + ga_6) + a_4\right], \tag{37}$$

$$\left(\frac{\partial U}{\partial\chi}\right)_{\rm LHS} = 3\Sigma_0^3z^9\left[-\frac{9}{14} + 16\frac{\Sigma_9}{\Sigma_0^3}\right] + 8\Sigma_0G_0^2z^{11}\left[-\frac{1}{3} + 10\frac{\Sigma_{11}}{\Sigma_0G_0^2}\right], \tag{38}$$

$$\left(\frac{\partial U}{\partial\chi}\right)_{\rm RHS} = \Sigma_0^3z^9\left[\frac{\sqrt{6}}{14}a_1 + 4a_3\right] + \Sigma_0G_0^2z^{11}\left[\frac{2\sqrt{6}}{27}a_1 + 2a_5\right], \tag{39}$$

$$\left(\frac{\partial U}{\partial G}\right)_{\rm LHS} = 6\Sigma_0^2G_0z^{10}\left[-\frac{3}{7} + 10\frac{G_{10}}{\Sigma_0^2G_0}\right] + 32G_0^3z^{12}\left[-\frac{1}{9} + 3\frac{G_{12}}{G_0^3}\right], \tag{40}$$

$$\left(\frac{\partial U}{\partial G}\right)_{\rm RHS} = \Sigma_0^2G_0z^{10}\left[\frac{\sqrt{6}}{14}(a_2 + ga_6) + 2a_5\right] \tag{41}$$

$$+ G_0^3z^{12}\left[\frac{2\sqrt{6}}{27}(a_2 + ga_6) + 4a_4\right]. \tag{42}$$

Altogether, from both the UV and IR limits, there are ten independent equations for the twelve parameters $a_0 - a_6$, Σ_9, Σ_{11}, G_{10}, G_{12}, and g. We take g as the free parameter to use as the rate of transition from small z to large z. The parameters in the potential are found to be

$$a_0 = \frac{3}{2}\frac{1}{6+\sin^2\theta}\left[120 + 62\sin^2\theta + 63\sqrt{6}g\sin^2\theta\right], \tag{43}$$

$$a_1 = -\frac{3\sqrt{6}}{4}\frac{1}{6+\sin^2\theta}\left[12 + 8\sin^2\theta + 9\sqrt{6}g\sin^2\theta\right], \tag{44}$$

$$a_2 = -\frac{\sqrt{6}}{4}\frac{1}{6+\sin^2\theta}\left[32+24\sin^2\theta+3\sqrt{6}g(9\sin^2\theta-2)\right], \tag{45}$$

$$2a_3\cos^2\theta + a_5\sin^2\theta = \frac{1}{24}\frac{1}{6+\sin^2\theta}\left[24+22\sin^2\theta+27\sqrt{6}g\sin^2\theta\right], \tag{46}$$

$$2a_4\sin^2\theta + a_5\cos^2\theta = \frac{1}{24}\frac{1}{6+\sin^2\theta}\left[20+22\sin^2\theta+3\sqrt{6}g(9\sin^2\theta-2)\right], \tag{47}$$

$$a_6 = -\frac{3}{2}. \tag{48}$$

The coefficients a_0, a_1, a_2 and a_6 are determined, while there are two equations for the three coefficients a_3, a_4 and a_5. That leaves a_5 as a free parameter, to be fit numerically, along with g, θ, G_0, Σ, and λ.

IV. NUMERICAL SOLUTION

Using the potential discussed above, we seek a numerical solution that simultaneously satisfies the UV and IR limits. We use Eqs. (12), (15), and (16), which allows for an additional term in the potential, ΔU, such that

$$\frac{\partial}{\partial\chi}\Delta U = \frac{\partial}{\partial G}\Delta U = 0, \tag{49}$$

which will be determined from the numerical solution.

The differential equations represent a stiff system, and treating the problem as an initial value problem leads to numerical instabilities. We treat it instead as a boundary value problem, using Dirichlet boundary conditions at both boundaries. A relaxation method is used in combination with input approximations for the background fields, which are then iterated to find a stable solution to the system with the given boundary conditions. Because the system is nonlinear, the solution found is not guaranteed to be unique.

The IR boundary is chosen to be sufficiently large to capture the infrared behavior and to give accurate Regge behavior for the large-n radial excitations of the mesons. The UV boundary should approach zero, but it cannot reach zero because of the singularity in the equations of motion. This becomes a problem because Eq. (12) allows constant and divergent terms,

$$\Delta\phi(z) = c_1 + c_2 z^{-1}. \tag{50}$$

Symbolically, these terms can be set to zero by enforcing the Dirichlet boundary condition $\phi(0) = 0$, but this is impossible to enforce numerically. A creative choice of UV boundary conditions can eliminate one, but not both, of these unwanted terms without affecting the chiral and glueball fields. The behavior of the numerical solutions suggests that the desired UV behavior is an unstable solution to the equations, and therefore difficult or impossible to find with this iterative method.

As an alternative to a direct solution, we parametrize the fields as follows:

$$\Psi(z) = \psi(z)_{UV} f(z) + \psi(z)_{\mathrm{IR}}(1-f(z)). \tag{51}$$

Here $f(z)$ is some function that transitions smoothly from 1 at small values of z to 0 at large z, while $\psi(z)_{xy}$ represents the known UV and IR limits of the fields ϕ, χ, and G. The switching functions need not be the same for each field. We choose

$$f_\phi(z) = e^{-(\beta_1 z)^{10}}, \tag{52}$$

$$f_\chi(z) = e^{-(\beta_2 z)^4}, \tag{53}$$

$$f_G(z) = e^{-(\beta_3 z)^5}. \tag{54}$$

The powers of the exponential are chosen to be greater than the known power-law behavior of the fields in the UV limit so as to not interfere with this behavior. The β_i will be determined by numerical fitting. The switching functions are not unique, but do allow for an accurate solution to the differential equations, as explained below.

The potential U, because it is a function of the background fields, will change depending upon the behavior of the fields. In particular, the additional ΔU term is numerically determined such that Eqs. (13) and (14) are solved by the background fields. A numerical nonlinear optimization routine, namely the interior point algorithm [22], is used to select the parameters that minimize the error in the finite-difference approximations to Eqs. (12), (15), and (16), thus ensuring that the parametrized fields are solutions to the background fields, within numerical tolerances. In this analysis, the fields ϕ, χ, and G solve Eqs. (12)–(16) to an accuracy of one part in 10^4.

The chiral condensate Σ is set using the Gell-Mann–Oakes–Renner relation:

$$(m_u + m_d)\Sigma = f_\pi^2 m_\pi^2. \tag{55}$$

Using $m_\pi = 139.6$ MeV, $f_\pi = 92$ MeV, and $m_u + m_d = 7.0$ MeV yields a value of $\Sigma = (286\ \mathrm{MeV})^3$.

In all, we have eight parameters to be determined numerically. In addition to obtaining solutions that solve the background equations, we also wish to achieve the best possible global visual fit to the vector and axial-vector meson spectra. We do not simply do a chi-squared fitting to the experimental data because the measurement error for

TABLE I. Best-fit parameters for the phenomenological model. The parameters λ, θ, and β_2 are chosen for the best visual fit to the ρ and a_1 data, with the rest set by minimizing the error in the equations of motion (12), (15), and (16).

$\lambda^{1/2}$	304 MeV	β_1	3.04 GeV
$G_0^{1/4}$	552 MeV	β_2	274 MeV
θ	1.44	β_3	558 MeV
g	3.20	a_5	1.63

the ground-state ρ meson is so much smaller than for the others that this would effectively act as the only constraint.

Three of the parameters are most phenomenologically relevant: λ, which controls the slope of the meson spectra in the large-n limit; θ, which controls the mass splitting between the a_1 and ρ mesons at large n; and β_2, which controls the location of the "bend" in the a_1 spectrum. For each set of these parameters, the other parameters are determined by a routine that minimizes the error in the equations of motion. The parameters found are shown in Table I.

The background fields that are obtained from this analysis are shown in Figs. 1–3. The asymptotic power-law behavior of the fields is evident in the linear portions of the log-log scale plots shown. The "transition" behavior is most evident in the dilaton because of the large value of β_1, which controls the value of z at which the field transitions from the UV limit to the IR limit.

We now analyze the "extra" term in the potential, ΔU. We obtain this term numerically by subtracting the right-hand side of Eq. (13) from its left-hand side. This term can be approximated numerically as a function of the dilaton field,

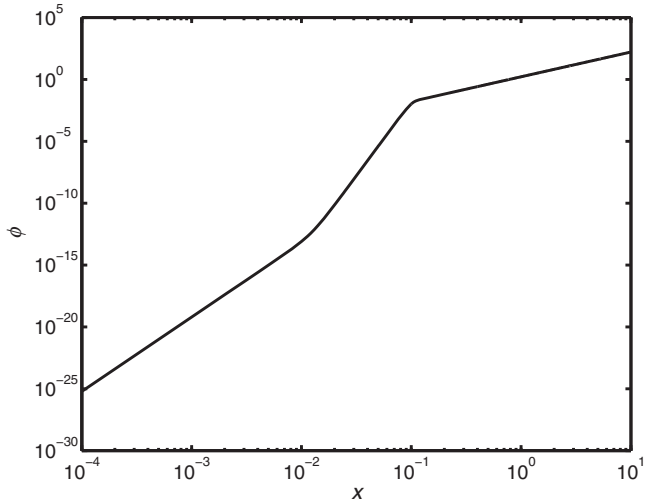

FIG. 1. A plot of the dilaton field Φ generated by the parametrization (52). The UV and IR asymptotic behavior is apparent. The coordinate x is a dimensionless rescaling of the conformal coordinate, $x = \sqrt{\lambda} z$.

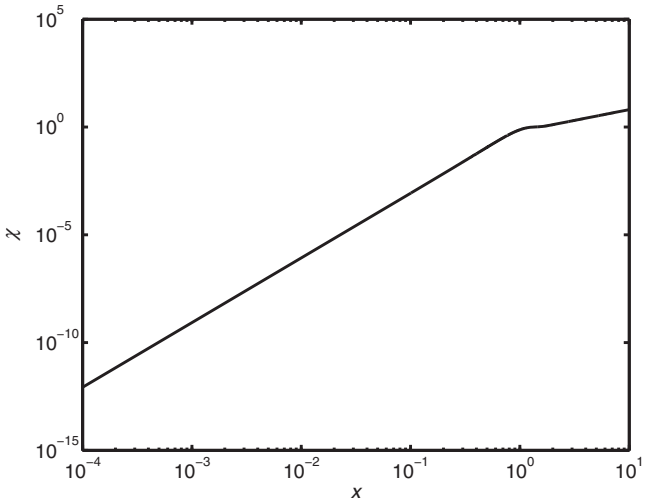

FIG. 2. A plot of the chiral field χ generated by the parametrization (53). The UV and IR asymptotic behavior is apparent, with a rapid transition between them. The coordinate x is a dimensionless rescaling of the conformal coordinate, $x = \sqrt{\lambda} z$.

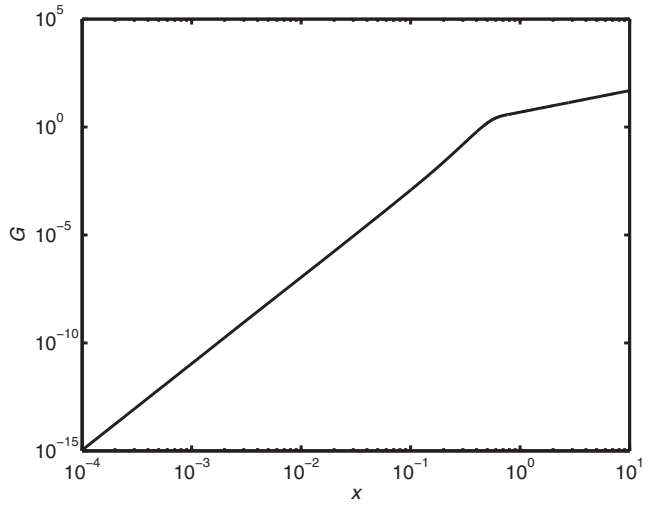

FIG. 3. A plot of the glueball field G generated by the parametrization (54). The UV and IR asymptotic behavior is apparent, with a rapid transition between them. The coordinate x is a dimensionless rescaling of the conformal coordinate, $x = \sqrt{\lambda} z$.

$$\Delta U(\phi) = \alpha_1 \phi^2 e^{-(\phi-\gamma_1)^2/\delta_1} + \alpha_2 \phi^2 e^{-(\phi-\gamma_2)^2/\delta_2}. \quad (56)$$

The best-fit values for these parameters are shown in Table II. The ΔU as a function of ϕ is shown in Fig. 4.

V. VECTOR AND AXIAL-VECTOR SPECTRA

To calculate the spectra of the radial excitations of the mesons, we examine the relevant terms from the string-frame action (1),

TABLE II. The dimensionless parameters for the fitting to ΔU.

α_1	-3.043×10^{1}	α_2	2.671×10^{-4}
γ_1	7.086×10^{-5}	γ_2	2.213×10^{-2}
δ_1	9.699×10^{-5}	δ_2	1.471×10^{-2}

$$\mathcal{S}_{\text{meson}} = -\frac{1}{16\pi G_5}\int d^5x\sqrt{-g}e^{-2\Phi}\text{Tr} \times \left[|DX|^2 + V_m(\Phi, X^2, \mathcal{G}) + \frac{1}{2g_5^2}(F_A^2 + F_V^2)\right]. \tag{57}$$

The 2×2 field X contains the scalar and pseudoscalar fields (S, π), as well as the VEV. We will use the exponential representation for the scalar field discussed in Ref. [8],

$$X_e = \left(S(x,z) + \frac{\chi(z)}{2}\right) I e^{2i\pi_e^a(x,z)t^a}, \tag{58}$$

where I is the 2×2 identity matrix.

We find the equations of motion for the various meson fields by varying the meson action. For the vector and axial-vector fields, we assume that the Kaluza-Klein modes are separable from the four-dimensional parts of the fields. The equation of motion in the axial gauge $\Psi_5 = 0$ is given by

$$-\ddot{\Psi}_n + \dot{\omega}\dot{\Psi}_n + M_\Psi^2(z)\Psi_n = m_{\Psi_n}^2\Psi_n, \tag{59}$$

where $\omega = 2\Phi(z) + \ln z$. The z-dependent mass term coefficient $M_V^2 = 0$ for the vector field, and

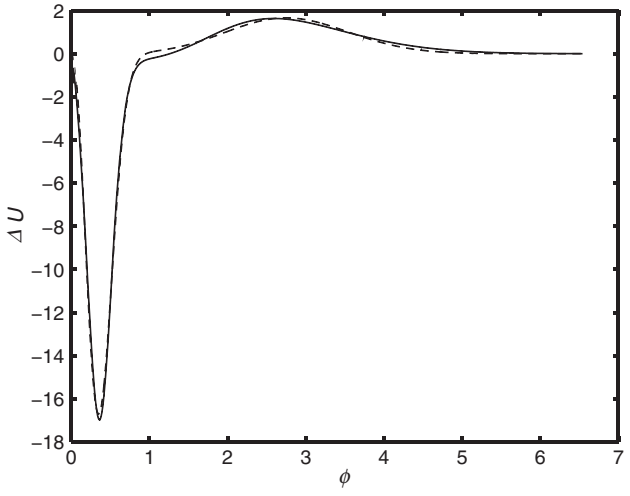

FIG. 4. Plot of the "extra" term in the potential, $\Delta U(\phi)$. The solid line represents the numerical result, while the dashed line is the fitting of Eq. (56) using the parameters of Table II.

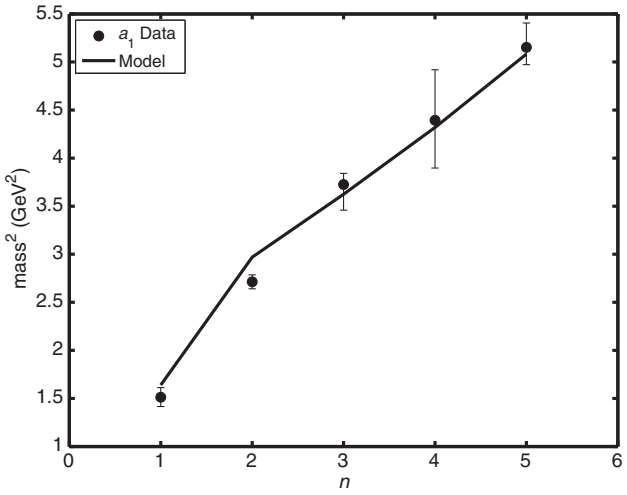

FIG. 5. Comparison of the predicted mass eigenvalues for the axial-vector sector with the experimental a_1-meson spectrum [23].

$$M_A^2 = \frac{g_5^2\chi^2}{z^2} \tag{60}$$

for the axial-vector field. The equation can be put in the Schrödinger form with the substitution $\Psi_n = e^{\omega/2}\psi_n$, resulting in

$$-\ddot{\psi}_n + \left(\frac{1}{4}\dot{\omega}^2 - \frac{1}{2}\ddot{\omega} + M_\psi^2\right)\psi_n = m_{\Psi_n}^2\psi_n. \tag{61}$$

These equations are analytically solvable in the IR limit,[1] but full analysis requires the use of a numerical shooting method to find the mass eigenvalues. The results for the axial-vector mesons are shown in Fig. 5 and in Table III. The results for the vector mesons are shown in Fig. 6 and in Table IV. This model finds a better phenomenological fit than the results presented in Ref. [7], particularly for the ground-state ρ meson. The scalar mesons are expected to mix with the scalar glueball field of this model; that analysis is deferred to a future publication.

VI. PSEUDOSCALAR SECTOR

When using the exponential representation for the scalar field, the terms from the potential do not contribute to the equations of motion for the pion field. This can be easily seen by noting that $|X_e|^n$ does not contain any terms involving the pion field π_e when n is even. We have required the potential to be an even function of X, so there are no such terms. This would seem to suggest that we use

[1]The analytical solution gives a large-n spectrum with a slope of 8λ, differing from the slope of 4λ found in other AdS/QCD models. This difference arises because of the $\exp(-2\Phi)$ prefactor in the action (1) compared to the prefactor of $\exp(-\Phi)$ used in other models [6,7]. This factor of 2 is compensated by the numerical value of λ shown in Table I, which is half the value used in other models. Thus, the notational choice does not affect the resulting meson spectra.

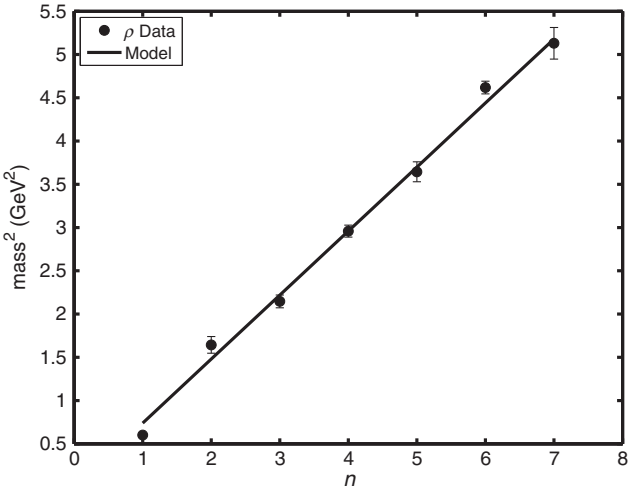

FIG. 6. Comparison of the predicted mass eigenvalues for the vector sector with the experimental ρ-meson spectrum. The included resonances are based upon Ref. [24] with the $n = 2$ resonance as suggested by Ref. [25].

the exponential representation to calculate the pion mass spectrum. However, as noted in Ref. [8], π_e is extremely sensitive to boundary conditions, and the numerical results are not reliable. For this reason, we seek to work with an equation of motion written in the linear representation.

For convenience, we begin by deriving the equations of motion in the exponential representation. Working in the axial gauge $A_z = 0$, we rewrite the axial meson field in terms of its perpendicular and longitudinal components: $A_\mu = A_{\mu\perp} + \partial_\mu\varphi$. Only the longitudinal component of the axial field, φ, contributes to the pion equations of motion. We use Eq. (57), keeping only the relevant terms,

$$\mathcal{L} = e^{-2\Phi}\sqrt{-g}\Big[\chi^2(\partial_\mu\pi_e\partial^\mu\pi_e + \partial_\mu\varphi\partial^\mu\varphi - 2\partial_\mu\pi\partial^\mu\varphi + \partial_z\pi_e\partial^z\pi_e) + \frac{1}{g_5^2}\partial_z\partial_\mu\varphi\partial^z\partial^\mu\varphi\Big]. \tag{62}$$

Varying with respect to φ yields

$$e^{2\Phi}\frac{d}{dz}\left(\frac{e^{-2\Phi}}{z}\dot{\varphi}\right) + \frac{g_5^2\chi^2}{z^3}(\pi_e - \varphi) = 0, \tag{63}$$

while varying π_e gives

$$\frac{e^{2\Phi}z^3}{\chi^2}\frac{d}{dz}\left(\frac{e^{-2\Phi}\chi^2}{z^3}\dot{\pi}_e\right) + m_n^2(\pi_e - \varphi) = 0. \tag{64}$$

It was shown in Ref. [8] that the equations of motion are equivalent under the substitution $\pi_e \to \pi_l/\chi(z)$, so we make the appropriate substitution and expand the equations:

$$-\ddot{\varphi} + \left(2\dot{\Phi} + \frac{1}{z}\right)\dot{\varphi} = \frac{g_5^2\chi}{z^2}(\chi\varphi - \pi_l), \tag{65}$$

$$-\ddot{\pi}_l + \left(2\dot{\Phi} + \frac{3}{z}\right)\dot{\pi}_l + \left(\ddot{\chi} - 2\dot{\chi}\dot{\Phi} - \frac{3\dot{\chi}}{z}\right)\frac{\pi_l}{\chi} = m_n^2(\pi_l - \chi\varphi). \tag{66}$$

We can put these equations into Schödinger-like form with the following substitutions:

$$\varphi = e^{\omega/2}\varphi_n, \tag{67}$$

$$\pi_l = e^{\omega_s/2}\pi_n, \tag{68}$$

with $\omega = 2\Phi + \ln z$ and $\omega_s = 2\Phi + 3\ln(z)$. This yields

$$-\ddot{\varphi}_n + \left(\frac{1}{4}\dot{\omega}^2 - \frac{1}{2}\ddot{\omega} + \frac{g_5^2\chi^2}{z^2}\right)\varphi_n = \frac{g_5^2\chi}{z}\pi_n, \tag{69}$$

$$-\ddot{\pi}_n + \left(\frac{1}{4}\dot{\omega}_s^2 - \frac{1}{2}\ddot{\omega}_s + \frac{\ddot{\chi}}{\chi} - \frac{2\dot{\chi}\dot{\Phi}}{\chi} - \frac{3\dot{\chi}}{z\chi} - m_n^2\right)\pi_n = -m_n^2\frac{\chi}{z}\varphi_n. \tag{70}$$

The dependence of these equations of motion on the scalar potential can be made explicit by using the background equation for the chiral field, written here in the string frame,

$$z^2\ddot{\chi} - 3z\dot{\chi}\left(1 + \frac{z\dot{\Phi}}{\sqrt{6}}\right) = m_X^2\chi + \frac{\partial U}{\partial\chi}. \tag{71}$$

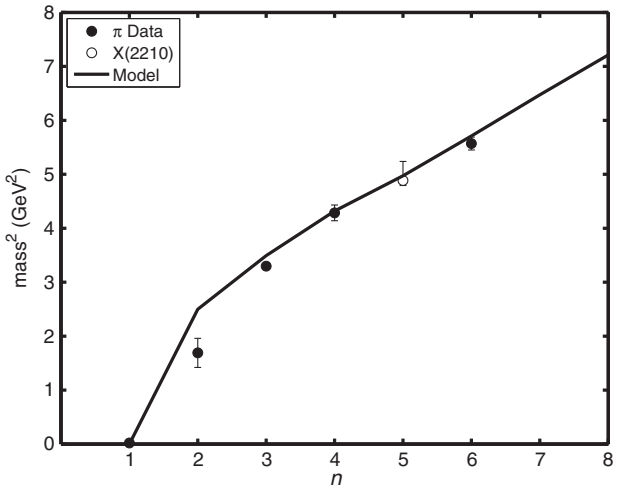

FIG. 7. Comparison of the predicted mass eigenvalues for the pseudoscalar sector with the experimental π-meson spectrum [23]. The states plotted here with $n = 4$ and $n = 6$ are identified as radial excitations of the pion only in the further states of the PDG. The unconfirmed state X(2210), with unknown quantum numbers, is plotted here as the $n = 5$ state of the pion.

Substituting, we can rewrite Eq. (70) as

$$-\ddot{\pi}_n + \left(\frac{1}{4}\dot{\omega}_s^2 - \frac{1}{2}\ddot{\omega}_s + \frac{m_X^2}{z^2} + \frac{1}{z^2}\frac{\partial U}{\partial \chi} - m_n^2\right)\pi_n = -m_n^2\frac{\chi}{z}\varphi_n. \tag{72}$$

The results are shown in Fig. 7 and in Table V. It should be emphasized that all parameters were previously determined, so these are truly predictions of the model. The states with mass 2070 and 2360 MeV are listed by the Particle Data Group (PDG) as further states, with less certainty assigned to them. We assume that these should be identified as the $n = 4$ and $n = 6$ states, leaving a vacancy at $n = 5$ for a state still to be observed in future experiments. On the other hand, the PDG has two further states listed as X(2210) with unknown quantum numbers, either of which could be the $n = 5$ state. We include this state in the figure and in the table, but it should be recognized that nothing in our work depends on this very speculative identification.

TABLE III. The experimental [23] and predicted values for the masses of the axial-vector mesons.

n	a_1 experimental (MeV)	a_1 model
1	1230 ± 40	1280
2	1647 ± 22	1723
3	1930^{+30}_{-70}	1904
4	2096 ± 122	2078
5	2270^{+55}_{-40}	2254

TABLE IV. The experimental and predicted values for the masses of the vector mesons. The included resonances are based upon Ref. [24] with the $n = 2$ resonance as suggested by Ref. [25].

n	ρ experimental (MeV)	ρ model
1	775.5 ± 1	860
2	1282 ± 37	1216
3	1465 ± 25	1489
4	1720 ± 20	1720
5	1909 ± 30	1923
6	2149 ± 17	2107
7	2265 ± 40	2276

TABLE V. The experimental [23] and predicted values for the masses of the pseudoscalar mesons. The states marked with a $*$ appear only in the further states of the PDG. The state marked with a † is an unconfirmed resonance X(2210) with unknown quantum numbers. Whether it really represents the $n = 5$ state is pure speculation.

n	π experimental (MeV)	π model
1	140	0
2	1300 ± 100	1580
3	1816 ± 14	1868
4	$2070 \pm 35^{*}$	2078
5	$2210^{+79\dagger}_{-21}$	2230
6	$2360 \pm 25^{*}$	2389
7	⋯	2544
8	⋯	2686

VII. CONCLUSION

In this paper we discussed the construction of a potential for the background fields of a soft-wall AdS/QCD model. We showed the limitation of a model that contains only the dilaton and chiral condensate fields, and suggested a solution by adding a glueball condensate to the model. We analytically constructed a general potential $U(\phi, \chi, G)$ that recovers the necessary asymptotic behavior of the background fields. Using this as a basis, we numerically constructed a potential that solves the selected background equations to within an accuracy of 10^{-4}. There is an additional allowed term in the potential, $\Delta U(\phi)$, that does not affect the equations that were used in the numerical procedure. This term was found numerically, and fit as a function of the dilaton field. These background fields were then used to find the spectra of the radial Regge mass spectra of the vector and axial-vector mesons. The model shows good phenomenological agreement with the experimental data for these spectra. With the parameters thusly determined, we computed the radial Regge mass spectrum for the pseudoscalar mesons (pions). Again there was good agreement, except for the most massive state, which perhaps should be identified with the radial quantum number $n = 6$ instead of $n = 5$.

The potential as constructed here is not guaranteed to be unique. If a different set of the background equations were chosen, the extra term would be expressed as a function of fields other than the dilaton. The parametrization in Eqs. (52)–(54) could also be chosen differently, resulting in a different potential but making little difference to the resulting meson spectra. Finally, terms can be added that do not affect the equations of motion at all, namely, terms which satisfy

$$\Delta U = \Delta\frac{\partial U}{\partial \phi} = \Delta\frac{\partial U}{\partial \chi} = \Delta\frac{\partial U}{\partial G} = 0. \tag{73}$$

This work demonstrates the construction of a potential for the background fields of a soft-wall AdS/QCD model that captures several key features of QCD observed through meson spectra. The radially excited states of the light mesons have linear Regge trajectories. Chiral symmetry is not restored for highly excited mesons, as seen in the constant mass splitting of the vector and axial-vector mesons. Working as we are in the limit of zero up- and down-quark masses, the pion is massless.

Future improvements to this model could include incorporating the light-quark masses by adding a linear term to

the UV limit of the chiral condensate field. The scalar mesons and glueballs will mix, and this analysis is left for future work. This potential also opens the possibility of exploring the thermal properties of a model that has the correct chiral symmetry breaking behavior.

ACKNOWLEDGMENTS

S. B. thanks Tony Gherghetta and Aleksey Cherman for useful discussions. S. B. also acknowledges Tom Kelley for the development of the code for calculating the pseudoscalar spectrum. This research is supported by the Department of Energy Office of Science Graduate Fellowship Program (DOE SCGF), made possible in part by the American Recovery and Reinvestment Act of 2009, administered by ORISE-ORAU under contract no. DE-AC05-06OR23100, by the U.S. Department of Energy (DOE) under Grant No. DE-FG02-87ER40328, and by a Doctoral Dissertation Fellowship from the University of Minnesota.

[1] J. M. Maldacena, Int. J. Theor. Phys. **38**, 1113 (1999).
[2] S. Gubser, I. Klebanov, and A. Polyakov, Phys. Lett. B **428**, 105 (1998).
[3] E. Witten, Adv. Theor. Math. Phys. **2**, 253 (1998).
[4] J. Erlich, E. Katz, D. T. Son, and M. A. Stephanov, Phys. Rev. Lett. **95**, 261602 (2005).
[5] L. Da Rold and A. Pomarol, Nucl. Phys. **B721**, 79 (2005).
[6] A. Karch, E. Katz, D. T. Son, and M. A. Stephanov, Phys. Rev. D **74**, 015005 (2006).
[7] T. Gherghetta, J. I. Kapusta, and T. M. Kelley, Phys. Rev. D **79**, 076003 (2009).
[8] T. M. Kelley, S. P. Bartz, and J. I. Kapusta, Phys. Rev. D **83**, 016002 (2011).
[9] P. Colangelo, F. De Fazio, F. Giannuzzi, F. Jugeau, and S. Nicotri, Phys. Rev. D **78**, 055009 (2008).
[10] L.-X. Cui, Z. Fang, and Y.-L. Wu, arXiv:1310.6487.
[11] C. P. Herzog, Phys. Rev. Lett. **98**, 091601 (2007).
[12] C. A. Ballon Bayona, H. Boschi-Filho, N. R. F. Braga, and Leopoldo A. Pando Zayas, Phys. Rev. D **77**, 046002 (2008).
[13] U. Gursoy, E. Kiritsis, L. Mazzanti, and F. Nitti, Phys. Rev. Lett. **101**, 181601 (2008).
[14] B. Batell and T. Gherghetta, Phys. Rev. D **78**, 026002 (2008).
[15] J. I. Kapusta and T. Springer, Phys. Rev. D **81**, 086009 (2010).
[16] U. Gursoy, E. Kiritsis, and F. Nitti, J. High Energy Phys. 02 (2008) 019.
[17] C. Csaki and M. Reece, J. High Energy Phys. 05 (2007) 062.
[18] D. Li and M. Huang, J. High Energy Phys. 11 (2013) 088.
[19] D. Li, M. Huang, and Q.-S. Yan, Eur. Phys. J. C **73**, 2615 (2013).
[20] S. He, S.-Y. Wu, Y. Yang, and P.-H. Yuan, J. High Energy Phys. 04 (2013) 093.
[21] M. Shifman and A. Vainshtein, Phys. Rev. D **77**, 034002 (2008).
[22] R. Byrd, J. Gilbert, and J. Nocedal, Math. Program. **89**, 149 (2000).
[23] J. Beringer *et al.* (Particle Data Group), Phys. Rev. D **86**, 010001 (2012).
[24] D. Bugg, Phys. Rep. **397**, 257 (2004).
[25] A. Bertin *et al.* (OBELIX Collaboration), Phys. Lett. B **414**, 220 (1997).